Hindawi
International Journal of Antennas and Propagation
Volume 2019, Article ID 7472186, 10 pages
https://doi.org/10.1155/2019/7472186

Research Article

Design and Validation of an Antipodal Vivaldi Antenna with Additional Slots

Marek Dvorsky,[1] **Harihara S. Ganesh**,[1] **and S. Sadhish Prabhu**[2]

[1] *Department of Telecommunications, Faculty of Electrical Engineering and Computer Science, VSB-Technical University of Ostrava, 17 listopadu 15, Ostrava, Czech Republic*
[2] *Department of Electronics and Communication Engineering, B.S.A Crescent Institute of Science and Technology, Vandalur, Chennai, India*

Correspondence should be addressed to Marek Dvorsky; marek.dvorsky@vsb.cz

Received 14 January 2019; Accepted 17 April 2019; Published 2 May 2019

Academic Editor: Miguel Ferrando Bataller

This paper introduces an improved shape of Antipodal Vivaldi Antenna from the normal schematic structure which yields a high radiation gain. We have designed and fabricated the improved structure of Antipodal Vivaldi Antenna with the help of new dielectric substrate ASTRA®MT77 material. We have chosen a unique substrate material to develop our novel Antipodal Vivaldi Antenna because most research has been done on commonly used materials like FR4, RT Duroid, etc. Moreover, ISOLA has significantly good electrical and nonelectrical properties as compared with other substrate materials. The results of the desired antenna were simulated through extensive simulations performed in CST Microwave Studio®. The characteristics of all the antenna parameters are clearly studied and we are successful to achieve closed results between designed as well as experimented Vivaldi Antenna. The simulated antenna achieved a maximum gain of more than 9 dBi whereas the experimental antenna reached around 7 dBi between the operating frequency range from 1 GHz to 13 GHz. The measured prototype antenna provides linear polarization with overall radiation efficiency of more than 90%.

1. Introduction

The Vivaldi Antenna was first described and characterized in 1979 by Gibson [1]. Later, the antipodal slot line suggested by Gazit [2] also referred to as symmetric double-sided slot line was constructed with microstrip feed as an input feed. To increase the performance of the antenna the slot line was used as a radiation mechanism and paired-strip improves the transition region. Noronha et al. [3] used this idea to construct a Vivaldi Antenna and have shown good results over a wide frequency range by maintaining a transition region from three to five wavelengths long distance to avoid a discontinuity between a feed and the radiating regions. The Antipodal Vivaldi Antenna (AVA) is a wideband and symmetric E and H plane that has been used extensively in radar applications [4–6], wireless communication applications [7, 8], and dual polarization applications [9, 10]. More recently, the Vivaldi Antenna has been identified as being suitable for Ultra Wide Band (UWB) applications [11]. With increasing interest in UWB as viable radio architecture, the Vivaldi Antenna has attracted interest due to its theoretically infinite bandwidth. It is a directional antenna with end-fire characteristics [12, 13].

2. Design and Optimization of Antipodal Vivaldi Antenna

2.1. Prototype Structure Description. The novel shape (see Figure 1) is designed on ASTRA®MT77 substrate [26] from ISOLA with a relative dielectric constant ϵ_r of 3.0 and a loss tangent of 0.0017, respectively. The AVA was initially constructed with a square microstrip patch length and width along with a microstrip transmission line mounted on a dielectric substrate as shown in Figure 2(a). As the radiating element of AVA is a balanced structure, hence it was mandatory to create a balun which provide a match between 50 Ω microstrip feed line and the antenna. This balun consists of 50 Ω microstrip to parallel plate transmission line, which tapers

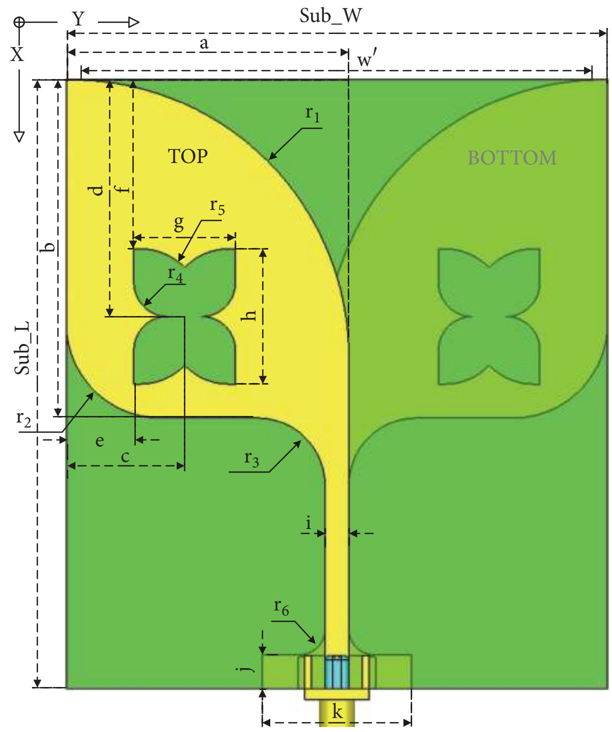

Figure 1: Designed structure of AVA.

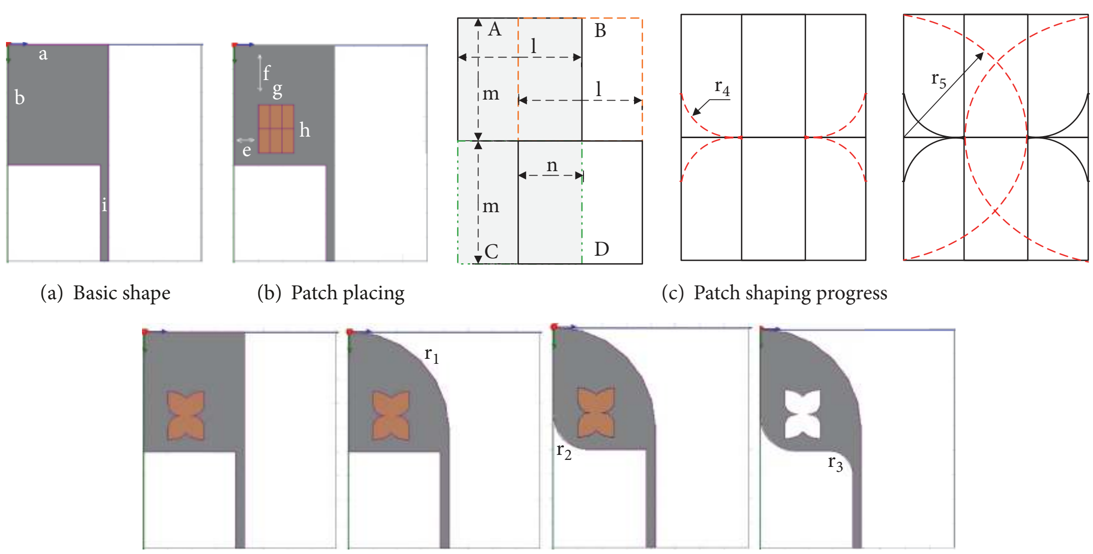

(a) Basic shape (b) Patch placing (c) Patch shaping progress

(d) AVA edges rounding to a final shape

Figure 2: Genesis procedure of AVA structure.

into a slotline configuration and later feeds the radiating element. The final antenna features were achieved with the help of the shape and placement of introduced slots in front and back side of AVA as shown in Figure 2(d). The final antenna design is presented by the CST Microwave Studio® (CST MWS) model in Figure 1. The square slots A–D (see Figure 2(c)) are placed on the AVA based upon trial and error method which is considered to be a heuristic approach.

This heuristics approach was used to match the overall impedance of the desired AVA. The front slots are fixed in the positions as seen in Figures 2(b) and 2(c) and Table 1: Box A (f, e, Sub_T), Box B $(f, e+l/2, Sub_T)$, Box C $(f+m, e, Sub_T)$, and Box D $(f+m, e+l/2, Sub_T)$. The bottom slots are consequently

Table 1: Antenna's dimensions and electrical parameters.

Sub_L	90.00 mm
Sub_W	80.00 mm
Sub_T	1.524 mm
a	41.75 mm
b	50.00 mm
c	17.50 mm
d	35.00 mm
e	10.00 mm
f	25.00 mm
g	15.00 mm
h	20.00 mm
i	03.50 mm
j	05.00 mm
k	22.00 mm
l	10.00 mm
m	10.00 mm
n	05.00 mm
w‘	78.50 mm
r_1	41.00 mm
r_2	14.00 mm
r_3	10.00 mm
r_4	05.00 mm
r_5	09.00 mm
r_6	03.70 mm
ϵ_r	03.00 [-]
Resistivity	1.33×10^7 MΩ·cm

placed on the directions: Box A (25, 55, 0), Box B (25, 60, 0), Box C (35, 55, 0), and Box D (35, 60, 0). By using the technical options like chamfer and blending, the shapes are properly constructed and later used for simulation.

The front and back shape contain two symmetric exponentially tapered patches placed on either side of the substrate. The exponentially tapered edge of the antenna is defined by the opening rate R and the two points $P_1(x_1, y_1)$ (the centre of the chamfer edge with the radius r_1) and $P_2(x_2, y_2)$ (the centre of the chamfer edge with radius r_2) [14, 15]. P_1 and P_2 are start and end points of the exponential taper. The design equations for the exponentially tapered edge are given by (1)–(3).

$$y = c_1 e^{Rx} + c_2 \tag{1}$$

where

$$c_1 = \frac{y_2 - y_1}{e^{Rx_2} - e^{Rx_1}}, \tag{2}$$

$$c_2 = \frac{y_1 e^{Rx_2} - y_2 e^{Rx_1}}{e^{Rx_2} - e^{Rx_1}}. \tag{3}$$

Given the lower cut-off frequency f_1, the width of the opening of the flared edges $w^‘$ should satisfy the below equation, respectively.

$$w^‘ = \frac{c}{f_1 \sqrt{\epsilon_r}}. \tag{4}$$

where c is the speed of the light, ϵ_r is the relative permittivity of used the substrate ASTRA®MT77. From (4) when $w^‘$ = 78.5 mm, the corresponding lower cut-off frequency can be calculated as 2.2 GHz.

We designed and fabricated the final prototype structure after perform extensive simulations and optimization process to obtain the maximum results of desired AVA in CST MWS. Final dimensions of designed AVA are tabulated in Table 1.

2.2. Steps to Achieve Prototype Structure. The top layer of the substrate was placed at position (0, 0, 0) (the left top corner; axis orientation: X vertically, axis Y horizontally) with the dimension Sub_L, Sub_W, Sub_T. The design procedure is summarised in Figures 2(a)–2(d). The rectangular slots A–D (10.00 mm × 10.00 mm) are curved with the help of CST MWS software options (see Figure 2(d)) to achieve a modified structure. The final planar patch is assembled from partly overlapped patches (A overlapped with B and C overlapped with D). The overlapping ratio n (5.00 mm) was obtained from optimization process in CST MWS. The same work flow has been followed to get a bottom structure with novel slots. As well as the top side, the normal shape of the bottom side has been modified with the help of CST MWS options to achieve a novel structure. Figures 3(a) and 3(b) show the final prototype of fabricated antenna.

3. Analysis and Measurements

The simulated antenna works in the frequency range between 3.7819 GHz to 4.7318 GHz, 5.6198 GHz to 7.6721 GHz, and 8.5281 GHz to more than 13 GHz. We successfully achieved a broadband communication for experimental antenna between the frequency range 5.592 GHz to more than 13 GHz and it covers an overall fractional bandwidth percentage of more than 100.54 % whereas there exists a lower bandwidth communication between 3.762 GHz and 4.814 GHz.

The reflection coefficient (Γ) and VSWR are also calculated with the help of mentioned formulas (5) and (6) by using return loss S11 measured values as a reference (see Figures 4 and 5). It has been observed that the measured VSWR of experimental antenna is less than 2 which covers the wide area between the operating frequencies ranges from 5.675 GHz to 13 GHz (see Figure 5).

$$\Gamma = 10^{S11/20} \tag{5}$$

$$\mathrm{VSWR} = \frac{1 + \Gamma}{1 - \Gamma} \tag{6}$$

(a) The top side

(b) The bottom side

Figure 3: Fabricated top and bottom structure of AVA with soldered SMA connector.

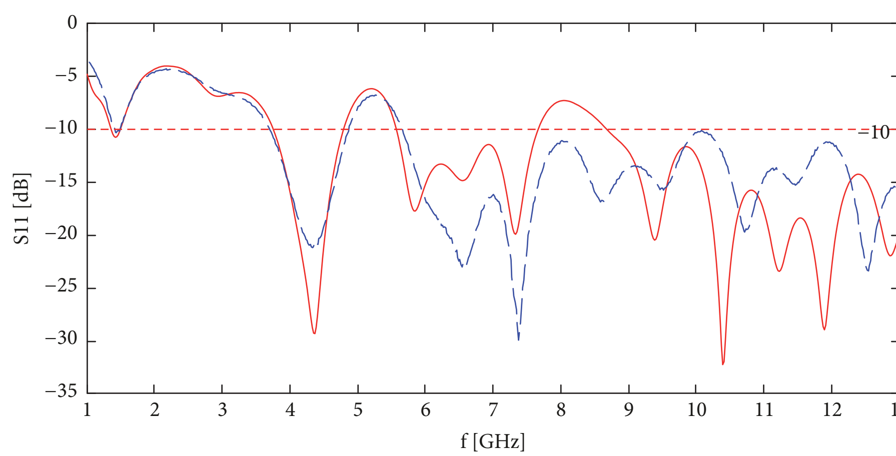

Figure 4: Simulation (full red curve) and measurement (dashed blue curve) comparison of S11.

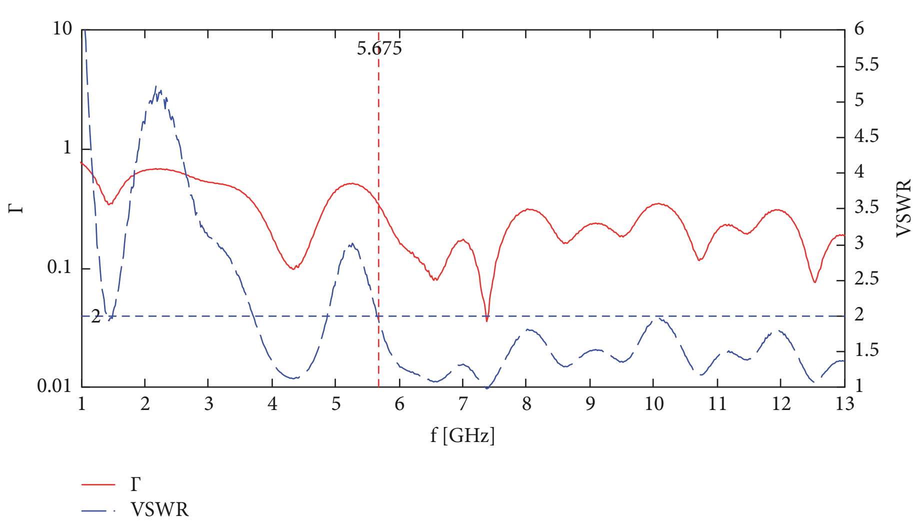

Figure 5: Reflection coefficient (full red curve) and VSWR (dashed blue curve) recalculated from the measurement values S11.

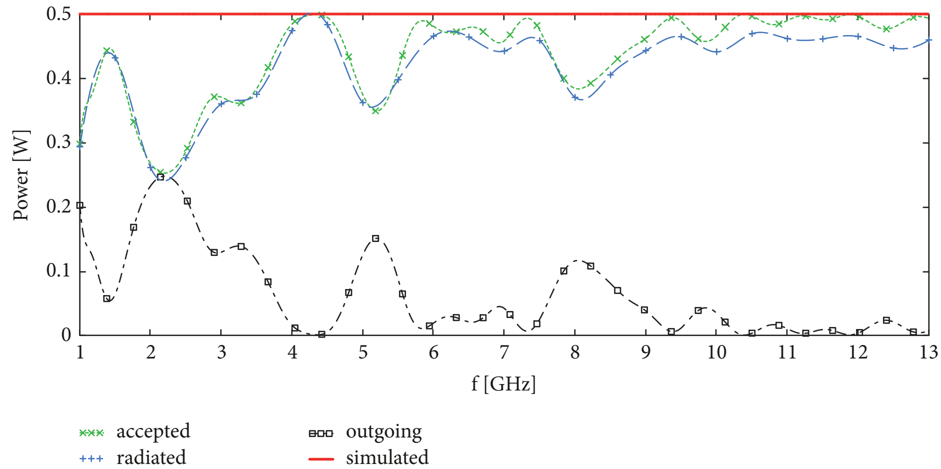

FIGURE 6: Simulation of power distribution: simulated 0.5 W (full red curve), radiated (dashed blue curve), accepted (dotted green curve), and outgoing (dash-dotted black curve).

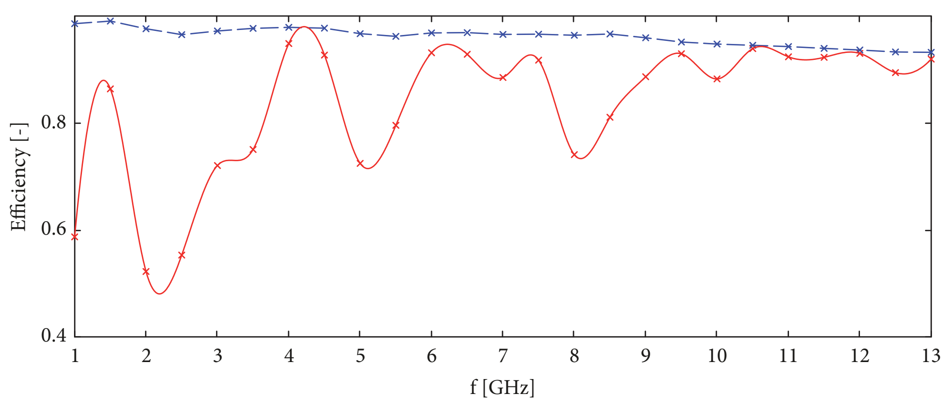

FIGURE 7: Total (full red curve) and radiation (dashed blue curve) efficiency simulated in CST-MW.

The total radiated power of an antenna is given by (7) where θ and φ are considered to be spherical coordinates. The standardized unit of R is W/Steradian. Hence the total radiated power is the spherical integral of R, which is given by [16] (see Figure 6).

$$\text{total radiated power} = \int_0^{2\pi}\int_0^{\pi} R(\theta,\varphi)\sin\theta d\theta\, d\varphi \qquad (7)$$

Figure 6 shows the power distribution of desired AVA. The effective radiated power is calculated with the help of basic formula (8).

$$\text{ERP} = \text{Input Power} + \text{Antenna Gain [dB]} \qquad (8)$$

From Figure 6 it is clear that the input power of desired antipodal antenna has an input power of 0.5 W, which has been derived from CST-MW [27], and the peak gain of simulated antenna is 9 dBi. Hence the effective radiated power is 4.5 W.

Figure 7 shows the overall total and radiation efficiency of prototype antenna derived from CST-MW. Radiation efficiency is defined as the ratio of radiated power to the input power of antenna whereas total antenna efficiency is described as the radiation efficiency multiplied by the impedance mismatch of the antenna and it is always less than the radiation efficiency. It is clear from Figure 7 that designed antenna covers the maximum radiation efficiency of more than 90% for the overall operating frequencies lying between 1 and 13 GHz.

The directivity diagrams on chosen frequencies have been measured in anechoic chamber with step of 1° (see Figure 8). The gain of measured antenna was calculated in E as well as H plane where the far-field distance of AVA is marked as 3 m. It is observed from Figure 9 that the simulated antenna achieved a maximum gain of 9.23 dB at 11.93 GHz whereas the measured antenna reached a peak gain of more than 7 dB at 12.58 GHz between the overall operating frequency ranges from 1 to 13 GHz, respectively.

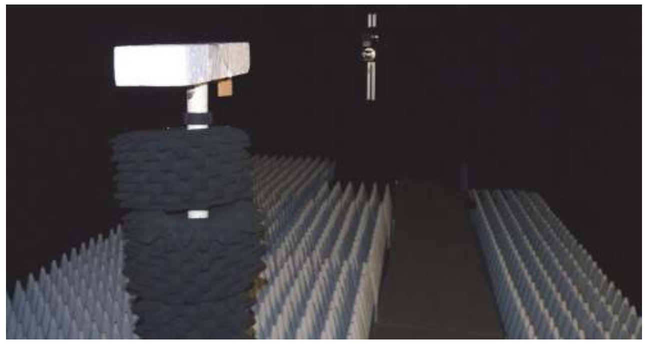

Figure 8: Measurement of far-field diagrams in anechoic chamber.

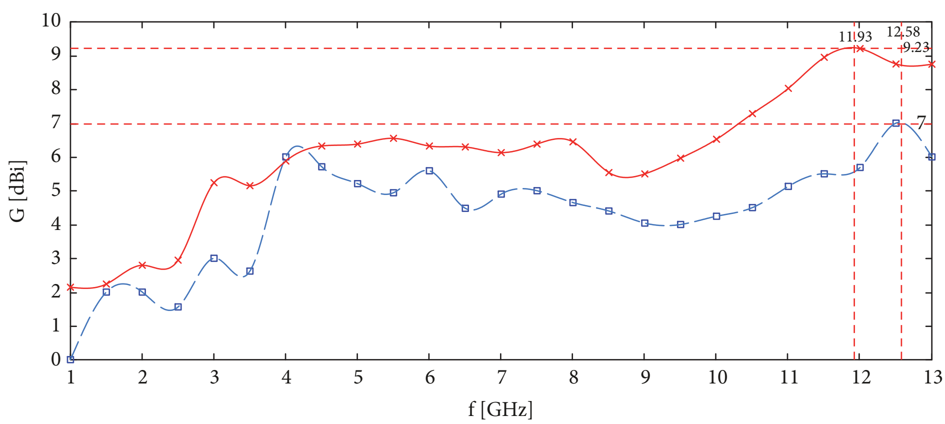

Figure 9: Simulation (full red curve) and measurement (dashed blue curve) comparison of antenna gain.

Figure 10 shows the 3D far-field simulation pattern of 11.93 GHz, where there exists a maximum gain (shown in Figure 9). The characteristics of antenna parameters at a desired operating frequency of 11.93 GHz are clearly studied. The realized peak gain is 9.252 dB. The radiation efficiency observed at a desired operating frequency of 11.93 GHz is 96.91% and the total antenna efficiency is 95.63%, respectively. The measured far-field radiation patterns of AVA structure at several typical frequencies (4 to 12 GHz) are presented in Figure 11. These patterns show that the desired prototype antenna provides low cross-polarization level at least 15 dB lower than copolarization level. The cross-polarization levels at other frequencies are very small, indicating good polarization purity. An improvement of front-to-back ratio and directivity is specifically obtained in E and H plane (see Table 2).

4. Conclusion

A portable miniaturized Antipodal Vivaldi Antenna has been constructed and measured. The experimental antenna achieved maximum return loss of -31 dB at an operating frequency of 7.368 GHz. The designed AVA exhibits satisfactory characteristics such as small size, fractional bandwidth, low cross-polarization of less than -15 dB, low side lobes as well as front/back ratio, realized peak gain <7 dB that operates within an overall frequency range from 5.592 GHz to 13 GHz, and stable radiation patterns over 4 GHz to 12 GHz which makes this antenna suitable for all the listed applications which are discussed in Table 3.

The proposed simulated antenna shows the notches around 5 GHz and 8 GHz whereas the practical measured antenna shows the notch at 5 GHz, respectively. It has been observed that when the distance between the slot centres is too far (i.e., $e \leq 10$ mm), antenna exhibits a wideband frequency notch, though it does not show the satisfied performances in the other frequencies. By decreasing the distance, the notch frequency shifts towards the lower frequency until $e = 10$ mm and bandwidth decreases. Also, however, when ($e \geq 10$ mm) the frequency shifts to the higher frequency where the notch bandwidth decreases, as it can be seen in Figure 4, the practical measurement shows better result at the distance ($e = 10$ mm) where the notch shifts to the lower frequency (from 4.9 to 5.6 ≈ 12.7%) and reduces the complete notch at higher frequency (8 GHz) and provides the UWB bandwidth from 5.592 to more than 13 GHz.

In future, the work can be extended to focus on design and development of Vivaldi Array Antenna with the help of corporate feed power divider to reduce maximum side

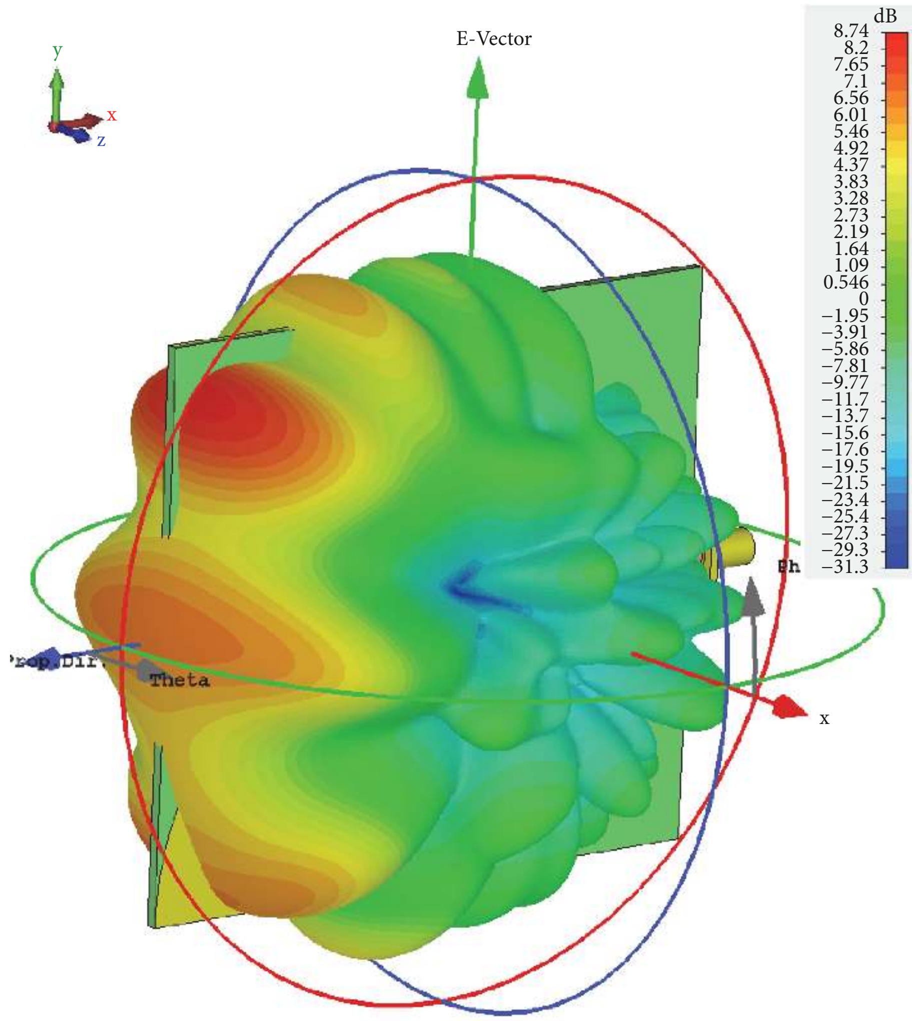

Figure 10: Far-field simulation at maximum gain frequency (11.93 GHz).

Table 2: Side lobes direction, front-to-back ratio and cross-polarisation.

f	Side Lobe				Front/Back		Cross Polarisation
	E		H		E	H	
[GHz]	Amp [dB]	Phase [°]	Amp [dB]	Phase [°]	[dB]	[dB]	[dB]
4	-0.28	167.98	-5.58	11.67	10.1	10.3	-05.3
5	-0.15	41.14	-9.44	47.02	12.0	12.1	-09.3
6	-0.23	-61.21	-15.72	53.26	10.7	12.2	-15.5
7	-0.25	176.12	-9.42	66.72	17.5	15.5	-09.2
8	-1.73	78.90	-7.48	166.77	19.3	11.2	-05.7
9	-4.08	-39.91	-16.38	-179.40	13.3	13.3	-12.3
10	-2.89	-122.88	-15.20	-134.02	14.2	7.2	-12.3
11	-2.92	132.30	-14.48	-170.99	16.0	14.5	-11.6
12	-4.17	24.41	-8.20	-149.83	24.1	19.2	-04.0

lobes as well as back lobes, narrow beam width along with high peak gain that can be used on different applications such as ground penetrating radar, radar cross-section reduction in stealth platform, and phased array applications.

Data Availability

The CST-MW Studio model and measurement data used to support the findings of this study are available from the corresponding author upon request.

Table 3: Comparative analysis of other Antipodal Vivaldi Antennas.

Ref. No.	Substrate Type	ϵ_r	tan δ	Dimension (L×W×H) [mm]	Frequency [GHz]	Gain [dBi]	Impedance Bandwidth	Radiation Efficiency	Cross Polarization	Application
our AVA	ISOLA	3.0	0.0017	090.00×080.00×1.524	01.0–13.0	≺ 7	3.608–4.904 GHz, 35% ≻ 5.592 GHz, ≺ 134.69%	≻ 90%	≺ -15.485 dB	applicable for all bellow application
[14]	FR4	4.30	0.0250	060.00×060.00×0.800	02.4–14.0	≺ 5	≺ 141%	NA	≺ -15.0 dB	UWB
[15]	FR4	4.40	0.0180	056.00×050.00×0.800	02.0–12.0	1.5–5.2	≻ 166%	60–83%	NA	UWB
[16]	PTFE	2.55	0.0020	046.00×045.00×0.800	03.1–10.6	≺ 5	NA	NA	≺ -14.5 dB	UWB
[17]	FR4	4.40	0.0020	040.16×042.56×1.400	03.1–10.6	≺ 5	NA	NA	≺ -20.5 dB	UWB
	RO30006	6.00	0.0020	039.40×034.60×1.000	03.1–10.6	≺ 5	NA	NA	≺ -20.5 dB	UWB
[18]	ARLON600	6.15	0.0030	190.01×128.01×1.575	00.8–12.0	6.32	163%	NA	NA	eng. harwesting
[19]	FR4	4.60	0.0200	040.00×040.00×1.600	3.01–06.8	5.9	NA	95%	NA	microwave imaging
[20]	FR4	4.30	0.0025	100.00×100.00×1.000	1.00–05.0	≺ 7.0	NA	NA	NA	microwave imaging
[21]	DURIOD5870	2.33	0.0012	060.50×040.00×0.787	4.73–25.0	4.0	405.4% at 5 GHz	NA	≺ 17 dB	UWB radars
[22]	FR4	4.40	0.0200	300.00×230.00×0.810	00.6–02.6	≺ 7	NA	98%	NA	LTE
[23]	NA	2.33	NA	274.00×282.00×1.575	0.40–09.8	10.0	184.3%	93%	NA	UWB
	NA	2.33	NA	161.25×140.00×1.575	0.83–09.8	10.0	175.8%	93%	NA	UWB
[24]	FR4B	2.65	0.0010	090.00×093.50×0.800	1.32–17.0	6.4	171%	NA	NA	UWB
[25]	Tacvonic CER10	10.0	NA	260.00×185.00×1.500	0.5–02.0	7.0	120%	NA	NA	UWB radars

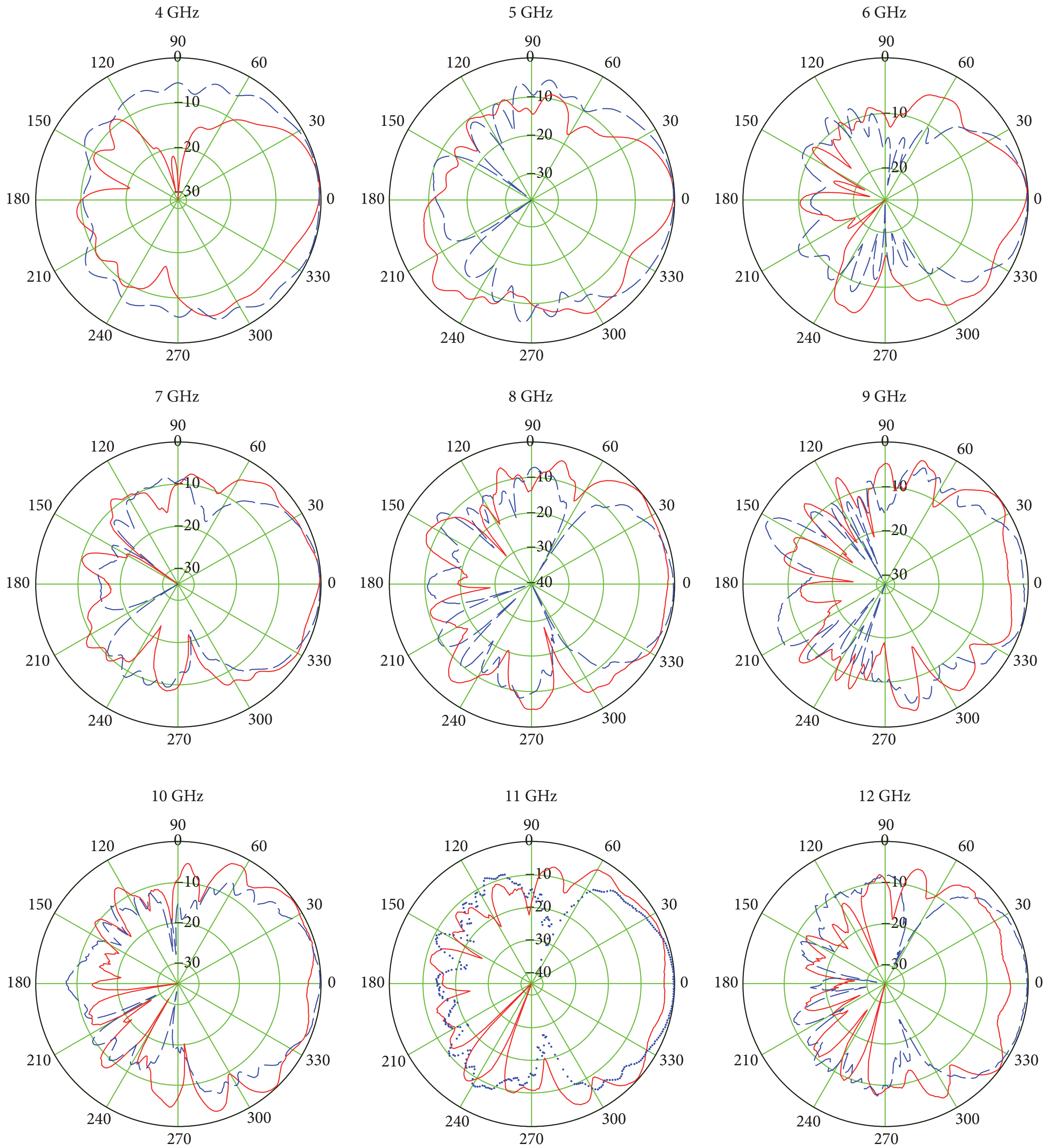

FIGURE 11: Measured far-field E (full red curve) and H (dashed blue curve) diagrams on chosen frequencies.

Conflicts of Interest

The authors declare that they have no conflicts of interest.

Acknowledgments

The research received a financial support from the SGS Grant no. SP2019/41, VSB-Technical University of Ostrava, Czech Republic. This article was also prepared within the frame of sustainability of Project no. CZ.1.07/2.3.00/20.0217 "*The Development of Excellence of the Telecommunication Research Team in Relation to International Cooperation*" within the frame of the operation programme "*Education for Competitiveness*" that was financed by the Structural Funds and from the state budget of the Czech Republic.

References

[1] P. J. Gibson, "The vivaldi aerial," in *Proceedings of the 9th European Microwave Conference*, pp. 101–105, Brighton, UK, September 1979.

[2] E. Gazit, "Improved design of the Vivaldi antenna," *IEE Proceedings Part H Microwaves, Antennas and Propagation*, vol. 135, no. 2, pp. 89–92, 1988.

[3] J. A. N. Noronha et al., "Designing antennas for UWB systems," *Microwaves and RF Journal*, pp. 53–61, 2003.

[4] G. Kwon, J. Park, D. Kim, and K. C. Hwang, "Optimization of a shared-aperture dual-band transmitting/receiving array antenna for radar application," *IEEE Transactions on Antennas and Propagation*, vol. 65, no. 12, pp. 7038–7051, 2017.

[5] K. Garenaux, T. Merlet, M. Alouini et al., "Recent breakthroughs in RF photonics for radar systems," *IEEE Aerospace and Electronic Systems Magazine*, vol. 22, no. 2, pp. 3–8, 2007.

[6] V. Mikhnev and P. Vainikainen, "Wideband Tapered-Slot antenna with corrugated edges for GPR applications," in *Proceedings of the 33rd European Microwave Conference, '03*, pp. 727–729, Munich, Germany, October 2003.

[7] G. R. Aiello and G. D. Rogerson, "Ultra-wideband wireless systems," *IEEE Microwave Magazine*, vol. 4, no. 2, pp. 36–47, 2003.

[8] N. Sobli and H. Abd-El-Raouf, "Design of a compact band-notched antenna for ultrawideband communication," in *Proceedings of the IEEE Antennas and Propagation Society International Symposium and USNC/URSI National Radio Science Meeting '08*, pp. 1–4, San Diego, Calif, USA, 2008.

[9] J. Lee, S. Livingston, and R. Koenig, "A low-profile wide band (5:1) dual-pol array," *IEEE Antennas and Wireless Propagation Letters*, vol. 2, pp. 46–49, 2003.

[10] J. Lee, S. Livingston, and R. Koenig, "Performance of a wideband (3–14 GHz) dual-pol array," in *Proceedings of the IEEE Antennas and Propagation Society Symposium, '04*, pp. 551–554, Monterey, Calif, USA, 2004.

[11] J. Bai, S. Shi, and D. W. Prather, "Modified Compact antipodal Vivaldi antenna for 4–50 GHz UWB application," *IEEE Transactions on Microwave Theory and Techniques*, vol. 59, no. 4, pp. 1051–1057, 2011.

[12] P. Wang, G. J. Wen, H. B. Zhang, and Y. H. Sun, "A wideband conformal end-fire antenna array mounted on a large conducting cylinder," *IEEE Transactions on Antennas and Propagation*, vol. 61, no. 9, pp. 4857–4861, 2013.

[13] G. W. M. Whyte, *Antennas for Wireless Sensor Network Applications [Ph.D. thesis]*, University of Glasgow, 2008.

[14] M. Kanagasabai, L. Lawrance, J. V. George et al., "Modified antipodal Vivaldi antenna for ultra wideband communications," *IET Microwaves, Antennas & Propagation*, vol. 10, no. 4, pp. 401–405, 2016.

[15] G. Pandey, H. Verma, and M. Meshram, "Compact antipodal Vivaldi antenna for UWB applications," *IEEE Electronics Letters*, vol. 51, no. 4, pp. 308–310, 2015.

[16] L. Yang, H. Guo, X. Liu, H. Du, and G. Ji, "An antipodal Vivaldi antenna for ultra-wideband system," in *Proceedings of the IEEE International Conference on Ultra-Wideband (ICUWB '10)*, pp. 1–4, Nanjing, China, 2010.

[17] A. Z. Hood, T. Karacolak, and E. Topsakal, "A small antipodal vivaldi antenna for ultrawide-band applications," *IEEE Antennas and Wireless Propagation Letters*, vol. 7, pp. 656–660, 2008.

[18] J. Schneider, M. Mrnka, J. Gamec, M. Gamcova, and Z. Raida, "Vivaldi antenna for RF energy harvesting," *Radioengineering*, vol. 25, no. 4, pp. 666–671, 2016.

[19] M. A. Syeed, M. Samsuzzaman, M. Z. Mahmud, and M. T. Islam, "A compact modified antipodal Vivaldi antenna for imaging application," in *Proceedings of the 3rd International Conference on Electrical Information and Communication Technology (EICT '17)*, pp. 1–5, Khulna, Bangladesh, 2017.

[20] L. Chen, C. Wang, H. Li, and S. Lan, "A miniaturized antipodal vivaldi antenna for microwave imaging," in *Proceedings of the International Symposium on Antennas and Propagation (ISAP '17)*, pp. 1-2, Phuket, Thailand, 2017.

[21] D. S. Cabral, L. Manera, and L. B. Zoccal, "Design and application of a compact UWB antipodal vivaldi antenna," in *Proceedings of the IEEE 17th International Conference on Ubiquitous Wireless Broadband (ICUWB '17)*, pp. 1–5, Salamanca, Spain, 2017.

[22] D. V. Navarro-Méndez, L. F. Carrera-Suárez, E. Antonino-Daviu et al., "Compact wideband vivaldi monopole for LTE mobile communications," *IEEE Antennas and Wireless Propagation Letters*, vol. 14, pp. 1068–1071, 2015.

[23] J. Y. Siddiqui, Y. M. Antar, A. P. Freundorfer, E. C. Smith, G. A. Morin, and T. Thayaparan, "Design of an ultrawideband antipodal tapered slot antenna using elliptical strip conductors," *IEEE Antennas and Wireless Propagation Letters*, vol. 10, pp. 251–254, 2011.

[24] Z. Wang, Y. Yin, J. Wu, and R. Lian, "A miniaturized CPW-fed antipodal vivaldi antenna with enhanced radiation performance for wideband applications," *IEEE Antennas and Wireless Propagation Letters*, vol. 15, pp. 16–19, 2016.

[25] F. Fioranelli, S. Salous, I. Ndip, and X. Raimundo, "Through-the-wall detection with gated FMCW signals using optimized patch-like and vivaldi antennas," *IEEE Transactions on Antennas and Propagation*, vol. 63, no. 3, pp. 1106–1117, 2015.

[26] ISOLA, "Astra MT77. In: Isola Group [online]. Chandler USA, 2019 [cit. 2019-04-23]," Available at: https://www.isola-group.com/wp-content/uploads/data-sheets/astra-mt77.pdf.

[27] CST STUDIO SUITE ® 2019, "Online Help, Power View," https://www.cst.com.